Macromolecules

pubs.acs.org/Macromolecules

Article

Janus-Type Dendrimers Based on Highly Branched Fluorinated Chains with Tunable Self-Assembly and ^{19}F Nuclear Magnetic Resonance Properties

Marta Rosati, Angela Acocella, Andrea Pizzi, Giorgio Turtù, Giulia Neri, Nicola Demitri, Nonappa, Giuseppina Raffaini, Bertrand Donnio, Francesco Zerbetto, Francesca Baldelli Bombelli,* Gabriella Cavallo,* and Pierangelo Metrangolo*

Cite This: *Macromolecules* 2022, 55, 2486−2496

Read Online

ACCESS | Metrics & More | Article Recommendations | Supporting Information

ABSTRACT: Tuning the self-assembly of dendritic amphiphiles represents a major challenge for the design of advanced nanomaterials for biomimetic applications. The morphology of the final aggregates, in fact, critically depends on the primary structure of the dendritic building blocks as well as the environmental conditions. Here we report a new family of fluorinated Janus-type dendrimers (FJDs), based on a short-chain and branched fluorinated synthon with 27 magnetically equivalent fluorine atoms, linked to bis-MPA polyester dendrons of different generations. Increasing size, flexibility, and number of peripheral hydroxyl groups, we observed a peculiar self-assembly behavior in bulk and in aqueous media as a consequence of the subtle balance between their fluorinated and hydrophilic portions. The lowest generation FJDs formed spherical nanoparticles in water, e.g., micelles, showing a single ^{19}F NMR peak with good signal-to-noise ratio and over time stability, making them promising as ^{19}F-MRI traceable probes. The highest generation FJD, instead, presented an interesting morphological transition from multilamellar dendrimersomes to tubules as a consequence of a subtle balance of intra- and intermolecular forces that compete at the interface. Interestingly, a reduction of the local mobility of CF_3 groups passing from dendrimersomes to tubules switches off the ^{19}F NMR signal. The transition mechanism has been rationalized by coarse-grain simulations as well as demonstrated by using cosolvents of different nature (e.g., fluorinated) that promote conformational changes, ultimately reflected in the self-assembly behavior. Short and branched fluorinated chains have here been demonstrated as new moieties for the design of FJDs with tunable self-assembly behavior for potential applications as biocompatible ^{19}F MRI probes in the construction of theranostic platforms.

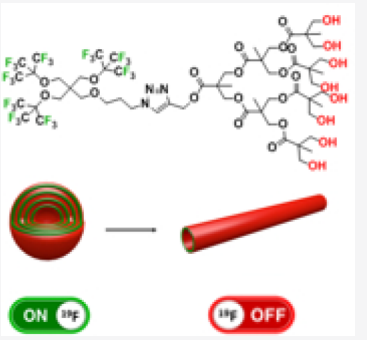

INTRODUCTION

Dendrimers are a class of highly structured three-dimensional macromolecules characterized by well-defined periodically branched structure, high monodispersity, and tunable size and shape.[1,2] Particularly interesting are Janus-type dendrimers (JDs), i.e., synthetic amphiphilic dendritic macromolecules bearing two domains of different polarity, which can also have different sizes.[3,4] These macromolecules self-assemble in water, giving rise to a wide variety of ordered morphologies such as micelles, tubular vesicles, cubosomes, disks, helical ribbons, and dendrimersomes.[5−7] A tailored balance between hydrophilic and hydrophobic portions allows the control of their self-assembly mode, which ultimately is responsible for the emergence of specific functions.[8−11] A powerful tool for tuning the self-assembly behavior of JDs and increasing their colloidal stability, also in biological media, is the introduction of fluoroalkyl groups in their molecular structure.[12−15] Formation of ordered arrangements is expected as a consequence of combined hydrophobicity and lipophobicity of fluoroalkyl moieties that induce segregation in both organic and aqueous environments (*fluorophobic effect*).[15,16] This phase separation has, for example, promoted generation of compartmentalized supramolecular structures with larger interfaces than their non-fluorinated analogues;[17,18] that is, vesicles are preferred over micelles and tubules over vesicles. Moreover, fluorination can also induce pronounced conformational changes,[19] as is the case of semi-fluorinated dendrons,[20−24] which can self-assemble in the bulk state into supramolecular columns exhibiting collective liquid crystalline behavior.[13,25−27]

JDs bearing linear fluorinated chains at their periphery have been extensively studied by Percec et al.,[5,7,28−32] who reported the formation of unilamellar and multilamellar dendrimer-

Received: February 3, 2022
Revised: March 13, 2022
Published: April 1, 2022

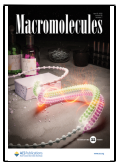

https://doi.org/10.1021/acs.macromol.2c00129
Macromolecules 2022, 55, 2486−2496

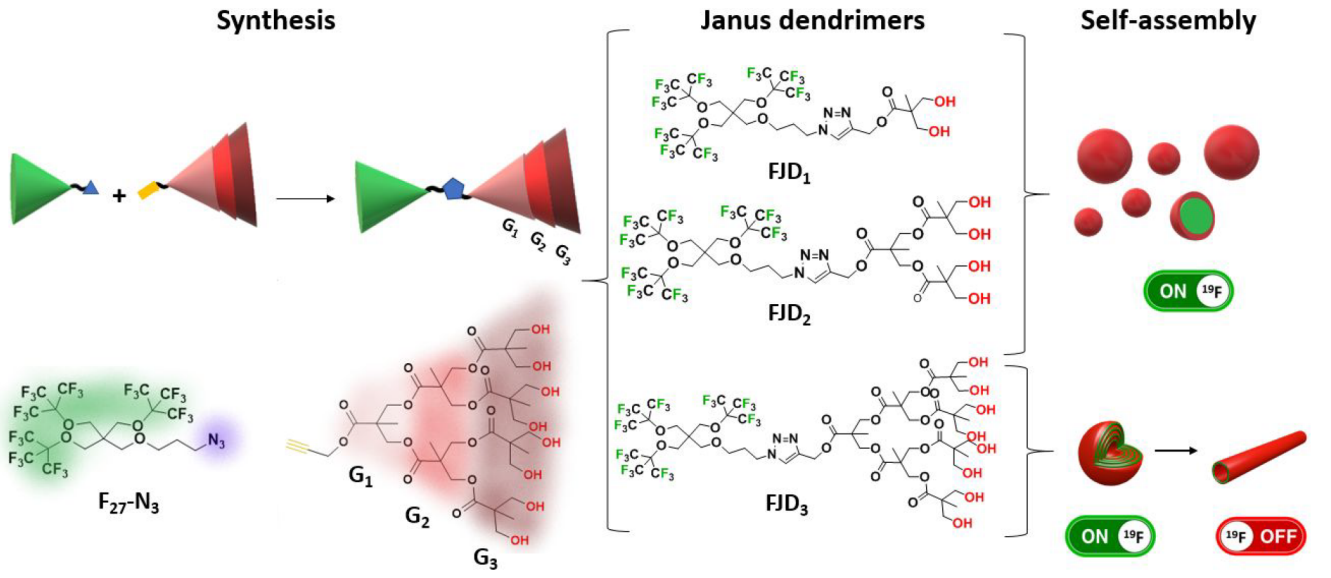

Figure 1. Fluorinated Janus-type dendrimers. The copper-catalyzed azide−alkyne cycloaddition (CuAAC) reaction allowed the orthogonal linkage of the fluorinated azide-terminating derivative (F_{27}-N_3) and alkyne terminating polyester dendrimers of generations I, II, and III (DG_1, DG_2, and DG_3). The three fluorinated Janus dendrimers (FJDs) obtained showed different magnetic properties at ^{19}F NMR depending on their self-assembly in aqueous media.

somes with bilayered structures arising from the interdigitation of the fluorinated chains.[7,29] Their bilayer thickness, comparable to that of biological membranes, together with their imaging capability via ^{19}F magnetic resonance imaging (MRI), renders them promising candidates for the development of theranostic systems and personalized drug therapies.[33−37] Indeed, permeability across fluorinated membranes is lower than their non-fluorinated analogues since the former are less dynamic than the latter, and exchange of components among micelles or vesicles is considerably slower.[17,38] In this regard, JDs containing perfluoropolyether chains were also used as nanocarriers for encapsulating polar guest molecules and generate stable water-in-fluorinated oil emulsions with possible application as polar nanoreactors in non-polar reaction media such as fluorous phases or supercritical CO_2.[38−40] However, to fully exploit the unique features offered by fluorinated JDs, there is a pressing need to design more sustainable fluorinated synthons.[41−43] In fact, perfluoroalkanes (PFAs) with chain lengths ≥6 carbon atoms are to be avoided for their bioaccumulative potential. On the other hand, PFAs with shorter chains do not lead to satisfactory results in terms of self-assembling performance.[44]

We have recently demonstrated that a multibranched superfluorinated thiol bearing perfluoro-*tert*-butoxyl groups is a valuable substitute for long-chain PFA thiols in the construction of omniphobic self-assembled monolayers[45] and stabilization of gold nanoclusters.[46] The unique design of the above-mentioned molecule allows multiplicity of equivalent fluorine atoms (27 F) for ^{19}F-MRI purposes, along with a stable and dense packing, due to the intrinsic tendency to crystallize of these branched fluorinated chains.[46,47] Moreover, the presence of four ether bonds in the core may hasten molecule degradation in the environment because of possible cleavage of these bonds in physiological conditions, thus overcoming PFA bioaccumulation issues.[45] A similar fluorinated branched structure was also applied by Yu et al. in the synthesis of nonassociative and water-soluble fluorinated amphiphiles.[48−51] Conversely, under the hypothesis that short-chain and multibranched fluorinated synthons may effectively drive JDs self-assembly in a manner similar to their linear counterparts, we targeted polyester dendrons of different generations bearing multiple perfluoro-*tert*-butoxyl groups. Interestingly, such macromolecules showed a tunable self-assembly behavior in aqueous media as a function of a subtle balance between fluorinated and hydrophilic domains (Figure 1). Coarse-grain simulations in combination with dynamic light scattering (DLS) and cryogenic transmission electron microscopy (cryo-TEM) experiments confirmed the formation of supramolecular structures of different morphologies and allowed rationalization of the molecular factors governing their self-assembly. In particular, the highest generation JD exhibited an interesting morphological transition from multilamellar dendrimersomes to tubules driven by a delicate balance of intra- and intermolecular forces that compete at the interface. Noticeably, the morphology of the resulting assemblies strongly impacts the intensity of their ^{19}F NMR signal, which is switched off on passing from dendrimersomes to tubules, as a likely consequence of the reduction of CF_3 local mobility. Interactions with cosolvents of different nature (i.e., fluorinated) have been demonstrated to promote conformational changes, which are ultimately reflected in the supramolecular organization. Overall, we propose here a new family of fluorinated JDs (FJDs), which show a versatile and tunable self-assembly behavior, paving the way for the development of functional supramolecular materials promising as ^{19}F-MRI probes for biological applications.

RESULTS AND DISCUSSION

Design and Synthesis of Fluorinated Janus Dendrimers (FJDs). The fluorinated JDs of generations from 1 to 3 ($\mathbf{FJD_{1-3}}$) were synthesized by using a click chemistry approach to connect hydrophilic and hydrophobic moieties. In particular, we exploited the copper-catalyzed azide−alkyne cycloaddition (CuAAC) reaction, which requires mild conditions and guarantees the orthogonal linkage of two

https://doi.org/10.1021/acs.macromol.2c00129
Macromolecules 2022, 55, 2486−2496

different molecular building blocks through the formation of a 1,4-disubstituted 1,2,3-triazole ring with good yields.[52] The azide derivative (F_{27}-N_3) (Scheme S1) was designed on the basis of the previously reported multibranched fluorinated thiol.[45] The synthesis occurred through a multistep reaction, starting from pentaerythritol as reported in the Supporting Information (Scheme S1). Its structure was confirmed by ATR-FTIR, ^{1}H, ^{13}C, and ^{19}F NMR measurements, and elemental analysis (Figures S1−S3).

FJDs$_{1-3}$ were synthesized following either a convergent or a divergent pathway (Schemes S2 and S3) according to the literature.[4] Both methodologies were highly efficient with yields higher than 70% in all cases. **FJDs$_{1-3}$** were fully characterized by ^{1}H, ^{13}C, and ^{19}F NMR, ATR-FTIR, and HRESI-MS spectroscopy. Formation of the sought amphiphilic dendrimers is evident from the presence in ^{1}H NMR spectra of the peak at about 8 ppm related to the proton of the triazole ring (Figure S4). Moreover, the presence of one single peak at around −71.5 ppm in the ^{19}F NMR spectra (Figure S5) confirms the presence of only one fluorinated compound and its purity. The successful formation of "clicked" dendrimers is also confirmed by ATR-FTIR spectra (Figures S6−S8) showing the disappearance of the bands at 2100 and 3300 cm^{-1} associated respectively with the N═N═N stretching of the azide F_{27}-N_3 and the C−H stretching of the alkyne-terminated dendrimeric precursors. Furthermore, the presence of C═O stretching vibrations at 1730 cm^{-1} and O−H stretching vibrations between 3600 and 3100 cm^{-1}, typical of polyester dendrons, together with C−F stretching and bending vibrations respectively at 1300 and 650 cm^{-1}, associated with the fluorinated moiety, confirm the linking between hydrophobic and hydrophilic portions.

Noncovalent Interactions Involved in the Formation of the Bulk Structure. **FJD$_1$** was crystallized by slow evaporation of an acetonitrile/toluene (1:10) solution. Single crystals suitable for X-ray diffraction analysis were measured at 100 K by means of synchrotron radiation. **FJD$_1$** crystallizes in the triclinic *P*-1 space group, with the unit cell containing two dendrimeric molecules related by a crystallographic inversion center (Figure 2a). Specifically, two facing **FJD$_1$** molecules share the π-surface of their triazole rings, the latter being stacked in antiparallel fashion. In addition to $\pi\cdots\pi$ stacking, the structure grows along the crystallographic *b*-axis thanks to a network of hydrogen bonds involving hydroxyl groups and triazole rings of neighboring molecules (Figure 2b). The incompatibility between fluorocarbon and hydrocarbon groups forces their segregation, producing a lamellar structure with a regular alternation of fluorinated and non-fluorinated regions (Figure 2c). Of note, the fluorocarbon layers are tightly packed, with an entangled network of weak F···F interactions that confers further stability to this supramolecular architecture. Overall, the high fluorine content of **FJD$_1$**, combined with the presence of polar groups, determines the typical self-assembly that is expected in these amphiphilic materials.

Thermal Behavior and Liquid Crystalline Properties. It is known for dendritic molecules that properties observed in bulk are often related to their self-assembling behavior in solution.[9,53] Therefore, small- and wide-angle X-ray scattering (SWAXS), polarized optical microscopy (POM), thermogravimetric analysis (TGA), and differential scanning calorimetry (DSC) were performed to study the molecular organization of **FJDs$_{1-3}$** in bulk. TGA performed in a nitrogen atmosphere showed the good thermal stability of all **FJDs**, as reported in

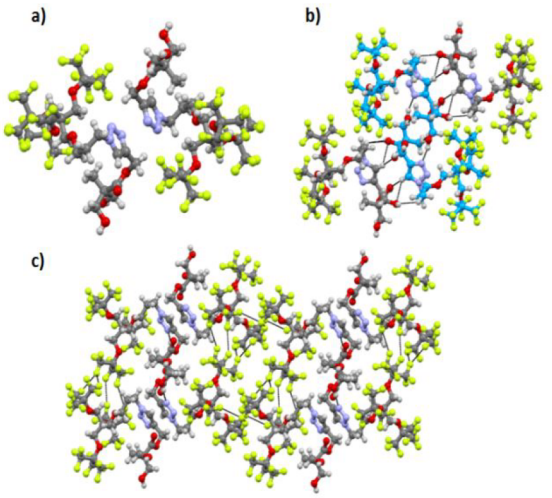

Figure 2. Single-crystal X-ray structure of FJD$_1$. (a) Dimers formed by antiparallel stacking. (b) Network of hydrogen bonds stabilizing the hydrocarbon regions formed by the packing of FJD$_1$ molecules. (c) Fluorine−fluorine interactions next to $\pi\cdots\pi$ stacking generate a layered structure. Color code: C, dark gray or light blue; H, light gray; F, yellowish-green; O, red; N, violet. Short contacts are depicted as black dotted lines.

Figure S9. For **FJD$_1$** and **FJD$_2$**, the onset decomposition temperature is at 206 and 248 °C, respectively, where a 5% weight loss occurs (T5%), and then degradation extends gradually up to 300 °C. **FJD$_3$** instead shows a two-step degradation at 170 °C (T5%) and 330 °C, suggesting that for the highest generation dendrimer thermal degradation starts from the outermost layer and then extends to inner layers.[54]

DSC and SWAXS analyses confirmed the crystallinity of **FJD$_1$** in the pristine state with a sharp melting peak at 91 °C, while on cooling from isotropic liquid, it froze into a glassy state (Figure S10). Loss of crystallinity was expected on increasing the dendritic generation according to the literature.[55] In fact, **FJD$_2$** is only partly crystalline in the pristine state. It melts at 72 °C to a quite fluid and non-birefringent mesophase with a low-energy (0.29 kJ/mol) and reversible transition around 104 °C to an isotropic liquid phase (Figure S11). The presence of only one single peak at low angles in SWAXS pattern precluded phase identification. However, the total absence of birefringence at POM suggested the formation of a cubic mesophase,[56,57] which is frozen in a glassy solid state on cooling to room temperature, as suggested from SWAXS (Figure S11a).

This liquid crystalline behavior can be explained considering the high tendency of fluorinated moieties to microsegregate.[25] Likely, the hydroxyl terminating segments tend to form compact double layers to compensate for the space requirement discrepancy with fluorinated segments, thus resulting ultimately in the fusion of strata into cubic network. Interestingly, SWAXS spectra show one halo at ca. 16° (i.e., 5.5 Å) that could be associated with molten CF_3 groups, while the second more extended halo of lesser intensity (ca. 10°) probably is related to average molecular distances (Figure S11a). **FJD$_3$** exhibits coexistence of several phases in the pristine state. DSC and POM revealed a broad transition at 86 °C, where a liquid suspension is formed, suggesting that only a partial melting has occurred, followed by a second broad transition at 100−110 °C, probably related to conformational rearrangements (Figure S12a). This is also confirmed by POM

https://doi.org/10.1021/acs.macromol.2c00129
Macromolecules 2022, 55, 2486−2496

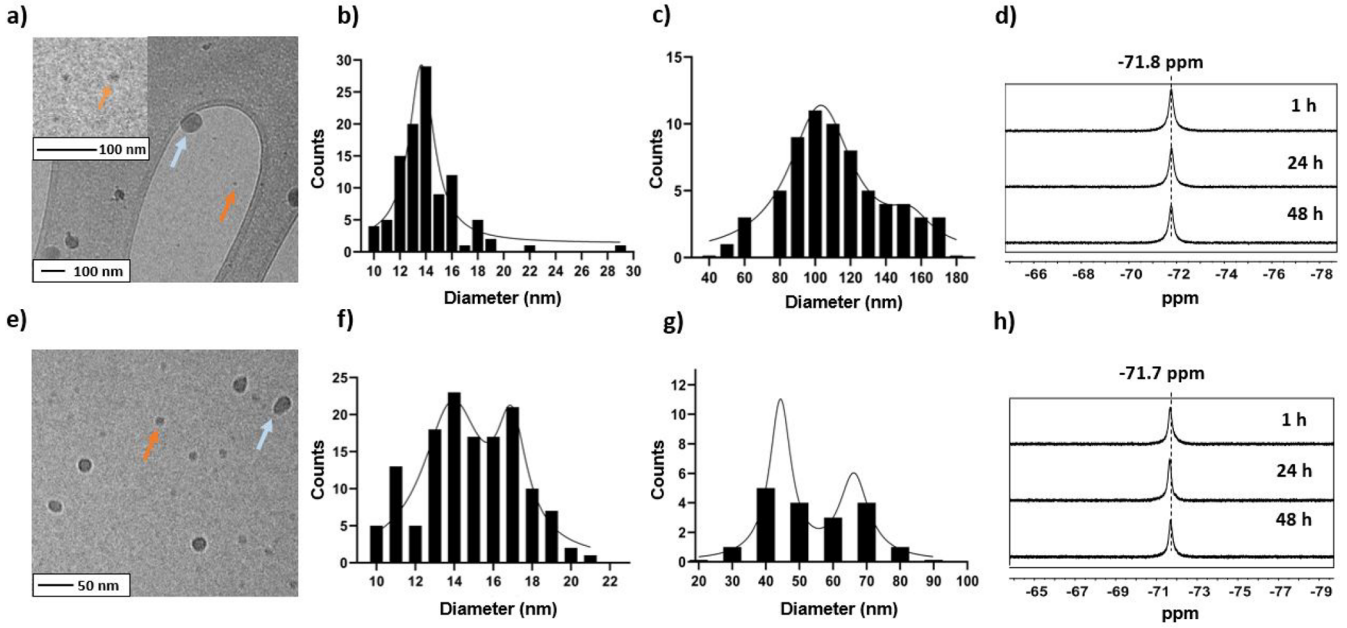

Figure 3. Self-assembly in water media of $\mathbf{FJD_1}$ (a–d) and $\mathbf{FJD_2}$ (e–h). (a) Cryo-TEM images show the formation of large spherical nanoparticles (light blue arrow) of around 100 nm of diameter and small nanoparticles, e.g., micelles (orange arrow) of 14 nm of diameter. (b) Size distribution profile of smaller nanoparticles from cryo-TEM images. (c) Size distribution profile of larger nanoparticles from cryo-TEM images. (d) ^{19}F NMR spectra over time (solvent: solution + D_2O 10% v/v). (e) Cryo-TEM images show the formation of large spherical nanoparticles (light blue arrow) of around 50 nm of diameter and small micelles (orange arrow) of 14 nm of diameter. (f) Size distribution profile of larger nanoparticles from cryo-TEM images. (g) Size distribution profile of smaller from cryo-TEM images. (h) ^{19}F NMR spectra over time (solvent: solution + D_2O 10% v/v).

and SWAXS pattern observed at 90 °C (Figure S12b,c) and hints at coexistence of different polymorphs with a different thermal behavior.[58,59] A similar behavior is reported in the literature for polyester dendritic amphiphiles of the same generation,[60] thus suggesting that increased mobility of the polyester chains can induce different molecular conformations, which are eventually responsible for the formation of different polymorphs.

Tuning the Self-Assembly of FJDs in Water. All synthesized **FJDs** can easily be dispersed in water by injection of their diluted solutions in ethanol (typically 10 mg/mL). This method has been reported to be extremely efficient for the formation of monodisperse dendrimersomes starting from amphiphilic JDs.[3] The resulting assemblies were analyzed over time by dynamic light scattering (DLS), cryogenic transmission electron microscopy (cryo-TEM), and ^{19}F NMR.

Cryo-TEM images of aged $\mathbf{FJD_1}$ and $\mathbf{FJD_2}$ dispersions showed the coexistence of two families of nanoparticles (Figure 3a, Figure S13 and Figure 3e, Figure S14, respectively). A statistical analysis of the analyzed images indicated that for $\mathbf{FJD_1}$ about 57% of the nanoparticles have an average diameter of 14 nm, while the remaining 43% show an average diameter of 105 nm (Figures 3b,c). In the case of $\mathbf{FJD_2}$, about 87% of the nanoparticles show an average diameter of 14 nm and only the 13% show a diameter of 52 nm (Figures 3f,g). These results were also coherent with DLS experiments as no significant changes were observed during sample aging in terms of size and polydispersity (Figure S15). ^{19}F NMR spectra of such formulations show a single resonance peak at around −72 ppm, and no significant changes were observed over time, thus confirming the colloidal stability of $\mathbf{FJD_1}$ and $\mathbf{FJD_2}$ (Figures 3d and 3h, respectively). A peculiar self-assembly behavior was instead observed for $\mathbf{FJD_3}$, which shows substantial changes in its aggregation mode upon aging. As schematically shown in Figure 4a, cryo-TEM images of the freshly prepared formulation revealed the presence of well-defined dendrimersomes of about 100 nm of diameter, composed of up to six layers, with an interlayer distance of 5 nm and a total layer width of 20 nm. Such dendrimersomes evolve over time forming structures of increasing complexity. Within 24 h at room temperature, vesicles start to interact and fuse with each other forming sheet-like structures, which gradually wrap around themselves giving rise to helical nanostructures, which eventually after 48 h evolve in tubule-like structures, as shown in Figure 4b. Simultaneously, a strong quenching of the ^{19}F NMR signal at −71.6 ppm was clearly observed at 48 h aging (Figure 4c). Because no precipitation occurred, quenching of the ^{19}F NMR signal would suggest, according to the literature,[61] a reduced mobility of CF_3 groups, probably related to the change in the morphology of the self-assembled structures.

The change in the aggregate morphology was also confirmed by DLS, where both polydispersity and hydrodynamic radius increased significantly at 48 h aging (Figure 4d). Interestingly, changing ethanol with trifluoroethanol (TFE), as cosolvent, the formation of tubular aggregates is prevented, and the presence of only spherical particles was confirmed by TEM. DLS and ^{19}F NMR did not change over time (Figure S16), confirming the stability of such dispersions. This suggests that $\mathbf{FJD_3}$ self-assembly is driven by a complicated pattern of forces that compete intra- and intermolecularly, in which the cosolvent plays a critical role, defining the final morphology of the supramolecular structures.

Considering the molecular structure of the three **FJDs**, we can assume that the interactions involved in their self-assembly are mainly fluorine–fluorine interactions, segregating fluorinated moieties from water, hydrogen bonding between polar headgroups and also with solvent, and stacking interactions

https://doi.org/10.1021/acs.macromol.2c00129
Macromolecules 2022, 55, 2486–2496

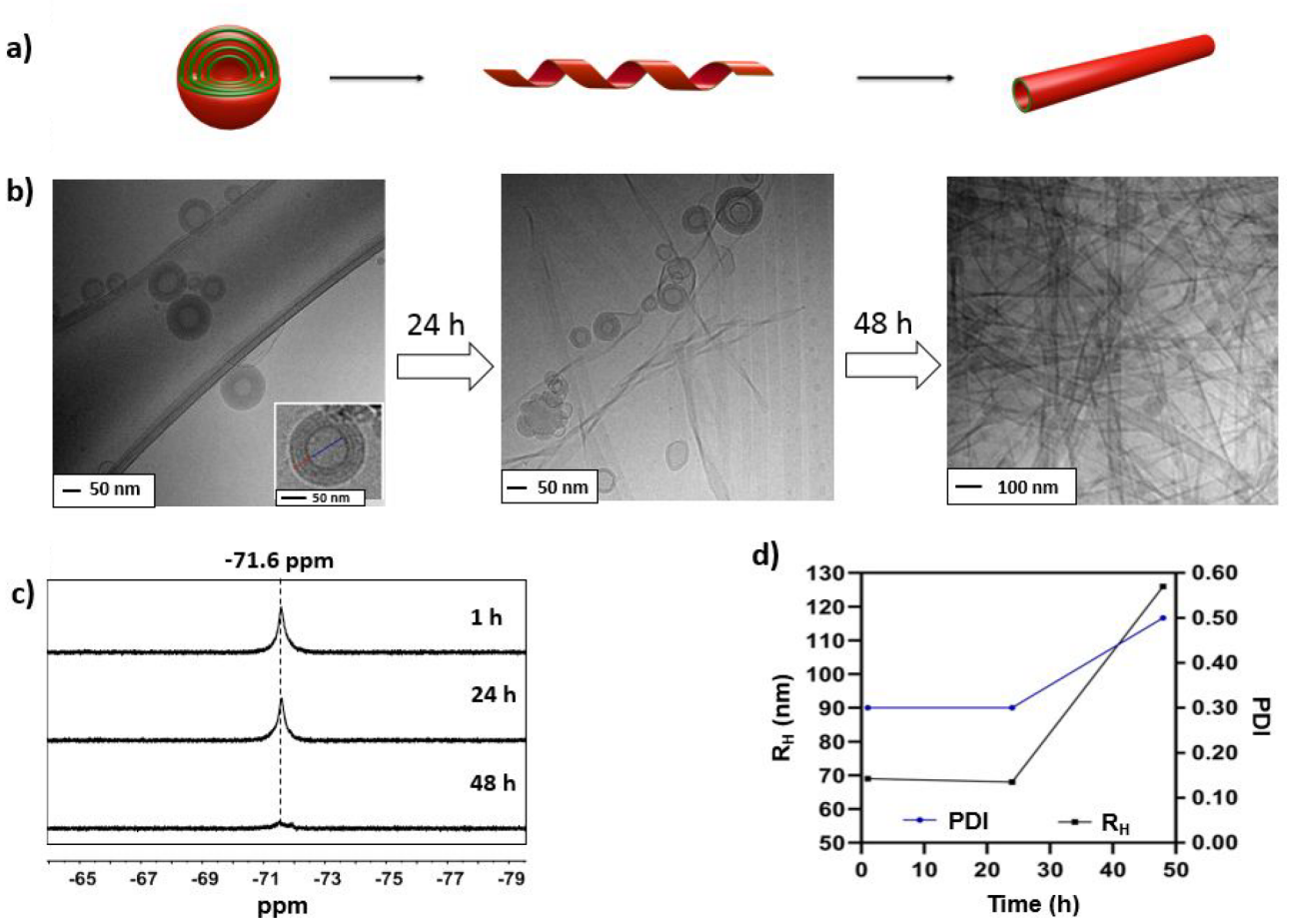

Figure 4. FJD_3 self-assembly in water media. (a) Cartoon scheme of the aggregates transition. (b) Cryo-TEM images showed the presence of multilamellar dendrimersomes that after 24 h fuse to form sheet-like structures, which finally form tubules after 48 h from sample preparation. Dendrimersomes are composed of an interlayer distance of 5 nm, and a total layer width of 20 nm (in red). (c) ^{19}F NMR spectra over time: after 48 h of aging there is the switching off of the signal (solvent: solution + D_2O 10% v/v). (d) DLS results: changes in the hydrodynamic radius (R_H, blue) and polydispersity (PDI, black) over time.

among triazole rings. It is thus reasonable to expect the formation of assemblies in which fluorine moieties are located in the inner strata, isolated from water, while hydroxyl groups are exposed on the external surface in contact with the aqueous medium. This is supported by the single crystal structure of FJD_1 that shows formation of fluorinated double layers as a consequence of the microsegregation of fluorinated segments, as also evident in FJD_3 multilayer dendrimersomes. Although the observed different self-assembly behavior could also be rationalized considering that while all **FJDs** contain the same fluorinated moiety, bis-MPA dendron increases in generation on going from FJD_1 to FJD_3. Probably, the morphology of the final supramolecular aggregate is regulated by a subtle balance between fluorinated and hydrophilic moieties and changing the hydrophilic/hydrophobic balance promotes morphological changes from spherical nanoparticles to tubules.

As suggested by cryo-TEM analyses and also supported by the literature for similar compounds,[62] FJD_3 multilamellar dendrimersomes observed in water/ethanol solutions might be metastable kinetic aggregates evolving to more thermodynamically stable tubular assemblies. This transition from aggregates with a higher curvature, i.e., dendrimersomes, to morphologies characterized by a lower curvature, i.e., tubules, produces an increased rigidity of the fluorinated chains, working as shut-off switch of the ^{19}F NMR signal.[61,63] This hypothesis is also supported by the high tendency of 27F group-containing molecules to crystallize, as reported elsewhere,[45,47,64−66] and is strengthened by the experimental evidence that changing ethanol with trifluoroethanol (TFE) as cosolvent prevents the formation of tubules, and only spherical nanoparticles are observed by TEM, while DLS and ^{19}F NMR do not show any changes over time (Figure S16). We speculate that TFE might completely change the interaction pattern at the interface interacting with the fluorinated moieties within the bilayer and rendering them more mobile (i.e., ^{19}F NMR signal on).

***In Silico* Modeling of FJD_3 Nanostructures.** A minimalistic model of coarse-grained interaction forces able to reproduce the experiments could shed light on the complex FJD_3 self-assembling process. Initially, we performed all-atom molecular dynamics simulations (AA-MD) of a single FJD_3 molecule and dimers dissolved in either water/ethanol or water/TFE solutions at different cosolvent concentrations. Figures 5a,b show two representative snapshots of the AA-MD of the monomer.

The AA-MD results of both monomer and dimer simulations were analyzed by means of three structural parameters: (i) the central dihedral angle, ϑ (Figure 5c), (ii) the radius of gyration, R_g (Figure 5d), and (iii) the radial distribution function (RDF) of the main chemical groups (Figure S17). The central dihedral angle of the single molecule

https://doi.org/10.1021/acs.macromol.2c00129
Macromolecules 2022, 55, 2486−2496

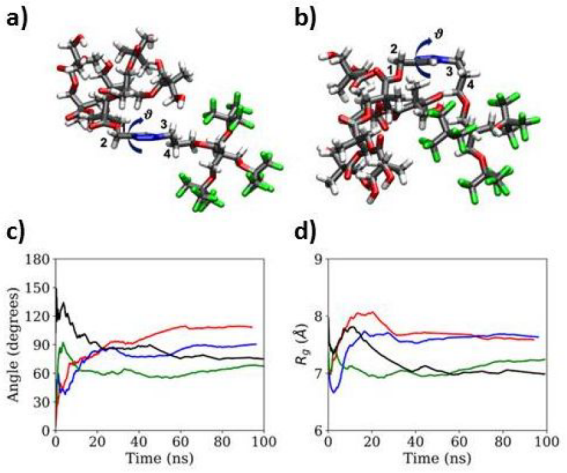

Figure 5. AA-MD simulations of a single FJD_3 molecule. Snapshots of (a) transoid and (b) cisoid conformations; fluorine atoms are green, carbon atoms gray, oxygen atoms red, hydrogen atoms white, and nitrogen atoms blue. The dihedral ϑ angle is also shown; the atom numbering is introduced to identify the dihedral angle. Solvent not shown to assist the eye. Summary of results in four solvent conditions; water (black line), 5% of ethanol in water (red line), 25% of ethanol in water (blue line), 5% of TFE in water (green line). (c) Plot of central dihedral angle of **FJD_3** vs time. (d) Plot of R_g vs time.

displays a certain amount of mobility, which reaches a limiting value in about 50 ns. In all the conditions, ϑ reaches an intermediate value between *trans* and *cis* conformations ($0° \leq \vartheta \leq 90°$ for *cis* structures, $90° \leq \vartheta \leq 180°$ for *trans* structures). Interestingly, ϑ and R_g values are on average higher in the presence of ethanol as cosolvent, indicating an unfolded transoid conformation for **FJD_3** in water/ethanol solutions. In the presence of 5% of TFE, instead, the dendrimer collapses in a cisoid conformation, probably due to specific F···F interactions with the cosolvent (Figures 5c,d). In fact, RDF analysis (Figures S17a–d) shows that TFE molecules are mainly located around the fluorinated end of **FJD_3**, showing a plethora of short contacts between carbonyl oxygens of **FJD_3** and hydroxyl group of TFE. AA-MD dynamics of the dimers did not show significant differences from those on the single molecules (details reported in Figures S18a–h and S19). Importantly, the unfolding of the dendrimer in the presence of ethanol could explain the lower mobility of the fluorinated portions, in agreement with ^{19}F NMR switch-off.

We have also run coarse-grained (CG) molecular dynamics simulations to gain insights into the **FJD_3** self-assembly process, with particular interest in its morphological transitions. Our minimal CG model has three different types of beads, as reported in Figure S20: (i) three CF beads with hydrophobic character representing the fluorinated end, (ii) two OA beads with hydrophilic character representing the polyester moiety, and (iii) three OC beads without a specific character, reproducing the linking group between the hydrophilic and hydrophobic ends. The associated parameters used in a dissipative particle dynamics (DPD) model are given in Table S3. Initially, CG simulations were set to reproduce **FJD_3** self-assembly in aqueous solutions. To rationalize the solvatophilic effect on self-assembled morphology, the interaction parameter ($a_{OA,S}$) between dendrimer hydrophilic beads (OA) and solvent (S) has been varied from 20 (higher hydrophilic interaction between dendrimer and solvent) to 35 (lower hydrophilic interaction between dendrimer and solvent). Cubic simulation boxes of $40r_c \times 40r_c \times 40r_c$ and $80r_c \times 80r_c \times 80r_c$ with periodic boundary conditions were applied, and the bead density was set to 3. Following Groot and Rabone,[67] the physical length scale r_c corresponds to 10 Å, resulting in boxes of 40 and 80 nm^3, respectively, the latter representing a reasonable size to accommodate the 60 nm diameter multilamellar dendrimersomes observed by means of cryo-TEM images. In this box, to reproduce the experimental concentration, a total of 1536000 beads were used (see the Supporting Information for details). As shown in Figure 6, referring to the largest boxes, at the highest hydrophilicity ($a_{OA,S} = 20$), we observed the formation of unilamellar hollow dendrimersomes and disk-like aggregates, while amphiphilic oligomers started to associate forming larger and multilamellar dendrimersomes upon reduction of the hydrophilicity. Finally,

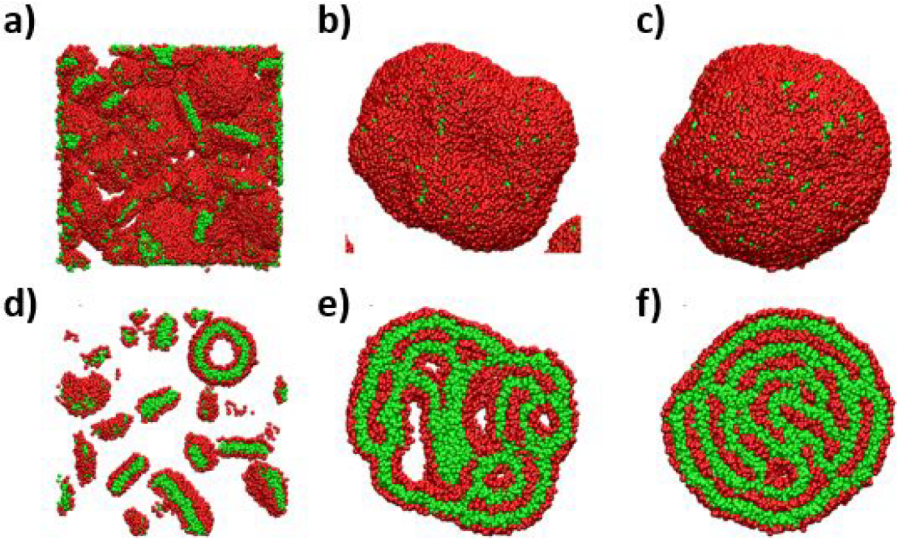

Figure 6. Snapshots of morphologies (upper row) and corresponding cross sections of the inner core (bottom row) of aggregates obtained with different $a_{OA,S}$ parameters: (a, d) $a_{OA,S} = 20$; (b, e) $a_{OA,S} = 30$; (c, f) $a_{OA,S} = 35$. Simulation box of dimensions $80r_c \times 80r_c \times 80r_c$. Color code: hydrophilic groups in red and hydrophobic groups in green. Water and OC beads are not represented here for the sake of clarity.

https://doi.org/10.1021/acs.macromol.2c00129
Macromolecules 2022, 55, 2486–2496

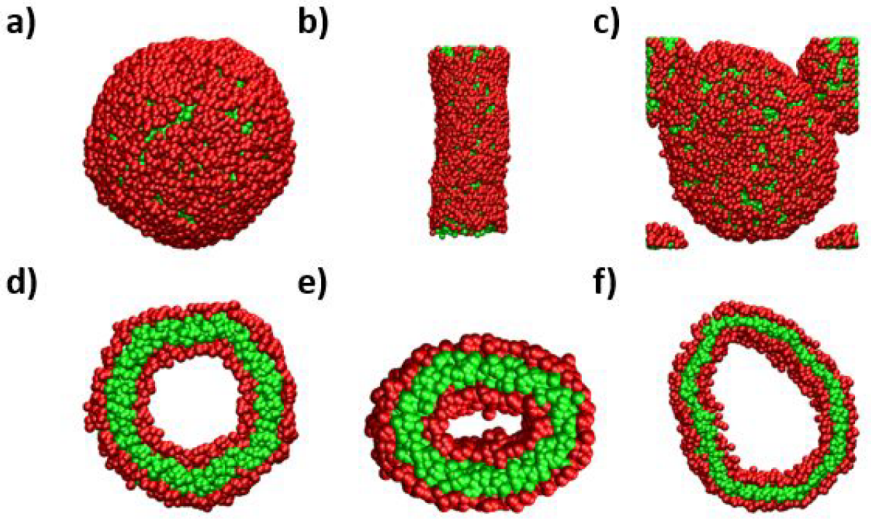

Figure 7. Snapshots of morphologies obtained in different conditions (upper row) and corresponding cross sections (bottom row) showing the hollow cores of the aggregates: (a, d) lowest ethanol concentration; (b, e) highest ethanol concentration; (c, f) TFE as a cosolvent. Color code: hydrophilic groups in red and hydrophobic groups in green. OC water and cosolvent beads are not represented to assist the eye.

at $a_{OA,S}$ = 35, the inner cavity closes with formation of dendrimersomes characterized by the presence of up to four layers (Figures 6e,f). These results demonstrate that the hydrophilic parameter governs the formation of dendrimersomes, in agreement with what observed in similar systems by Arai et al.[68] The results of the smaller box are similar; the major difference is the number of layers and the size of the dendrimersomes (Figures S21a–f).

A time evolution study of the transformation of the aggregates into dendrimersomes obtained with the largest box for $a_{OA,S}$ = 30 was also performed by calculating the mean aggregation number (N_{agg}) (Figure S22). Figure S22 shows snapshots taken at different times of the dendrimersomes formation process, starting from an initial random distribution. The mean aggregation number abruptly increases with time (vertical lines of Figure S22). At short simulation time (200 ns) (Figure S23b), **FJD$_3$** molecules start aggregating into disk-like structures, which fold into dendrimersomes with a mechanism that resembles the movement of a hand palm forming a fist. After 300 ns, single dendrimersomes start coalescing into larger spherical particles, gradually embedding nearby smaller structures (represented by Figures S23c–f). At longer simulation times (>1400 ns), spherical particles form dendrimersomes merging into large multiporous structures, which ultimately form multilayered systems (Figures S23g–j) with a mechanism already described by Chang et al.[69]

Additionally, we performed a new set of simulations that explicitly included the cosolvents (EtOH or TFE) to unravel their role in the time-dependent morphological changes experimentally observed for **FJD$_3$**.[70−72] The cosolvents were represented as two beads, where one is hydrophobic and the other hydrophilic. The cosolvent beads were labeled EO and EC for ethanol and TO and TC for TFE; coarse-grained interaction parameters are reported in Table S3. We performed three new CG simulations: two at a high concentration of cosolvent and an additional one at a lower EtOH concentration. Cubic simulation boxes of $40r_c \times 40r_c \times 40r_c$ dimensions with periodic boundary conditions were applied with bead density set to 3 with a total number of 192000 beads (as described in detail in the Supporting Information). Figure 7 reports the final morphologies of the aggregates obtained for the three simulations, which are in good agreement with cryo-TEM results. In particular, at the lowest ethanol concentration, unilamellar dendrimersomes were observed, characterized by a large central hollow core, with a diameter of about 22 nm and a double-layer thickness of about 6 nm. As ethanol concentration increases, elongated tubular aggregates are formed, with a central cavity of about 12 nm. In particular, it is evident that ethanol molecules fully cover the external and internal walls of the tubule, forming inner and outer coatings. Contrarily, the presence of TFE as cosolvent promotes the formation of dendrimersomes, characterized by a very large cavity of about 32 nm. A deeper inspection of the dendrimersome double layer showed the presence of interdigitated TFE molecules in the hydrophobic stratum, contrary to what observed in ethanol (Figure S24).

CONCLUSIONS

Here we reported the synthesis and structural characterization of a new family of fluorinated Janus-type dendrimers, **FJDs**, bearing a short-chain multibranched fluorinated moiety with 27 magnetically equivalent fluorine atoms linked to bis-MPA polyester dendrons of different generations. All synthesized **FJDs** are easily dispersed in aqueous solutions by injection of their diluted solution in ethanol, forming self-assembled nanostructures with a morphology dependent on a subtle balance between hydrophilic and hydrophobic portions in the molecule.

For the lowest generation dendrimers (**FJD$_1$** and **FJD$_2$**), spherical nanoparticles identified by cryo-TEM and characterized by a high colloidal stability (DLS) are observed. Associated ^{19}F NMR spectra to these nanostructures show a single peak with a good signal-to-noise ratio making them traceable by ^{19}F MRI. On the contrary, the highest generation derivative, **FJD$_3$**, self-assembles into multilamellar dendrimersomes displaying a morphological transition into tubular structures after 48 h of aging. Simultaneously, the switching-off of the ^{19}F NMR signal is observed, indicating lower mobility of the fluorine atoms as a consequence of a higher rigidity of the fluorinated portions. Interestingly, substituting

https://doi.org/10.1021/acs.macromol.2c00129
Macromolecules 2022, 55, 2486−2496

ethanol with trifluoroethanol as cosolvent, the transition to tubules is prevented and ^{19}F NMR spectra do not change over time.

Computational studies allowed rationalization of the molecular factors governing the self-assembly of the highest generation dendrimer showing that depending on the nature of the cosolvent, **FJD$_3$** assumes different conformations. In fact, with TFE as cosolvent, **FJD$_3$** mostly visits bent structures with the fluorinated moiety and hydrophilic groups arranged in a sort of cisoid conformation, probably driven by specific F···F interactions with the cosolvent. On the contrary, with ethanol as cosolvent, **FJD$_3$** adopts an unfolded transoid conformation. These conformational changes are at the basis of the complex self-assembly behavior seen for **FJD$_3$** in aqueous media. In particular, in the presence of ethanol as cosolvent, the fluorinated moieties of **FJD$_3$**, confined in the inner strata of the nanostructures, are more strongly interdigitated by F···F noncovalent interactions, while polyester chains are involved in hydrogen bonds with the cosolvent, driving the formation of longitudinal stable aggregates. In the presence of a fluorinated cosolvent(TFE), instead, F···F interactions between dendrimer and TFE provide a higher solvation of **FJD$_3$**, stabilizing a cisoid conformation and preventing the formation of tubular structures. A stronger interdigitation among **FJD$_3$** fluorinated moieties in the tubular structures also justifies a lower mobility of the CF_3 groups with a significant reduction of their ^{19}F NMR signal.

In conclusion, short and branched fluorinated chains are here demonstrated as novel moieties for the design of JDs with tunable self-assembly behavior and functional properties. This novel design paves the way toward a plethora of applications from transport of gases to ^{19}F MRI tracking. The ability of similar fluorinated JDs to deliver genetic material is currently under patenting[73] and will be reported elsewhere.

■ ASSOCIATED CONTENT

Supporting Information

The Supporting Information is available free of charge at https://pubs.acs.org/doi/10.1021/acs.macromol.2c00129.

Additional experimental and computational details, analytical graphs, references, Tables S1−S4, and Figures S1−S23 (PDF)

■ AUTHOR INFORMATION

Corresponding Authors

Francesca Baldelli Bombelli − *Laboratory of Supramolecular and Bio-Nanomaterials (SupraBioNanoLab), Department of Chemistry, Materials, and Chemical Engineering "Giulio Natta", Politecnico di Milano, 20133 Milan, Italy;* orcid.org/0000-0001-8138-9246; Email: francesca.baldelli@polimi.it

Gabriella Cavallo − *Laboratory of Supramolecular and Bio-Nanomaterials (SupraBioNanoLab), Department of Chemistry, Materials, and Chemical Engineering "Giulio Natta", Politecnico di Milano, 20133 Milan, Italy;* orcid.org/0000-0001-6387-9014; Email: gabriella.cavallo@polimi.it

Pierangelo Metrangolo − *Laboratory of Supramolecular and Bio-Nanomaterials (SupraBioNanoLab), Department of Chemistry, Materials, and Chemical Engineering "Giulio Natta", Politecnico di Milano, 20133 Milan, Italy;* orcid.org/0000-0002-7945-099X; Email: pierangelo.metrangolo@polimi.it

Authors

Marta Rosati − *Laboratory of Supramolecular and Bio-Nanomaterials (SupraBioNanoLab), Department of Chemistry, Materials, and Chemical Engineering "Giulio Natta", Politecnico di Milano, 20133 Milan, Italy*

Angela Acocella − *Dipartimento di Chimica "G. Ciamician", Alma Mater Studiorum - Università di Bologna, 40126 Bologna, Italy*

Andrea Pizzi − *Laboratory of Supramolecular and Bio-Nanomaterials (SupraBioNanoLab), Department of Chemistry, Materials, and Chemical Engineering "Giulio Natta", Politecnico di Milano, 20133 Milan, Italy;* orcid.org/0000-0002-4180-9151

Giorgio Turtù − *Dipartimento di Chimica "G. Ciamician", Alma Mater Studiorum - Università di Bologna, 40126 Bologna, Italy*

Giulia Neri − *Laboratory of Supramolecular and Bio-Nanomaterials (SupraBioNanoLab), Department of Chemistry, Materials, and Chemical Engineering "Giulio Natta", Politecnico di Milano, 20133 Milan, Italy*

Nicola Demitri − *Elettra Sincrotrone Trieste, 34149 Basovizza, Trieste, Italy;* orcid.org/0000-0003-0288-3233

Nonappa − *Faculty of Engineering and Natural Sciences, Tampere University, FI-33720 Tampere, Finland;* orcid.org/0000-0002-6804-4128

Giuseppina Raffaini − *Department of Chemistry, Materials, and Chemical Engineering "Giulio Natta", Politecnico di Milano, 20133 Milan, Italy*

Bertrand Donnio − *Institut de Physique et Chimie des Materiaux de Strasbourg - IPCMS, UMR 7504 - CNRS, Université de Strasbourg, F-67034 Cedex 2 Strasbourg, France;* orcid.org/0000-0001-5907-7705

Francesco Zerbetto − *Dipartimento di Chimica "G. Ciamician", Alma Mater Studiorum - Università di Bologna, 40126 Bologna, Italy;* orcid.org/0000-0002-2419-057X

Complete contact information is available at: https://pubs.acs.org/10.1021/acs.macromol.2c00129

Funding

F.B.B., G.C., and P.M. are thankful to the NEWMED project, ID 1175999 (funded by Regione Lombardia, POR FESR 2014−2020), and to the project NiFTy funded by MIUR (PRIN2017, no. 2017MYBTXC).

Notes

The authors declare no competing financial interest.

Deposition Number 2009095 contains the supplementary crystallographic data for this paper. These data are provided free of charge by the joint Cambridge Crystallographic Data Centre and Fachinformation zentrum Karlsruhe Access Structures service www.ccdc.cam.ac.uk/structures.

■ ACKNOWLEDGMENTS

Nonappa acknowledges the provision of facilities at the Nanomicroscopy Centre at Aalto University (OtaNano) and Photonics Research and Innovation (PREIN) flagship. B.D. thanks the CNRS and University of Strasbourg.

■ ABBREVIATIONS

AA-MD, all-atom molecular dynamics; ATR-FTIR, attenuated total reflectance Fourier-transform infrared spectroscopy; bis-MPA, 2,2-bis(hydroxymethyl)propionic acid; CG, coarse grained; cryo-TEM, cryogenic transmission electron microscopy; CuAAC, copper-catalyzed azide−alkyne cycloaddition; DLS, dynamic light scattering, DPD, dissipative particle dynamics; DSC, differential scanning calorimetry; EtOH, ethanol; **FJD$_1$**, fluorinated Janus dendrimer of generation 1; **FJD$_2$**, fluorinated Janus dendrimer of generation 2; **FJD$_3$**, fluorinated Janus dendrimer of generation 3; HRESI-MS, high-resolution electrospray ionization mass spectrometry; **JDs**, Janus dendrimers; MRI, magnetic resonance imaging; NMR, nuclear magnetic resonance spectroscopy; PFCs, perfluorocarbons; POM, polarized optical microscopy; RDF, radial distribution function; SWAXS, small- and wide-angle X-ray scattering; TEM, transmission electron microscopy, TFE, 2,2,2-trifluoroethanol; TGA, thermal gravimetric analysis.

■ REFERENCES

(1) Astruc, D.; Boisselier, E.; Ornelas, C. Dendrimers Designed for Functions: From Physical, Photophysical, and Supramolecular Properties to Applications in Sensing, Catalysis, Molecular Electronics, Photonics, and Nanomedicine. *Chem. Rev.* **2010**, *110* (4), 1857−1959.

(2) Sowinska, M.; Urbanczyk-Lipkowska, Z. Advances in the Chemistry of Dendrimers. *New J. Chem.* **2014**, *38* (6), 2168−2203.

(3) Percec, V.; Wilson, D. A.; Leowanawat, P.; Wilson, C. J.; Hughes, A. D.; Kaucher, M. S.; Hammer, D. A.; Levine, D. H.; Kim, A. J.; Bates, F. S.; Davis, K. P.; Lodge, T. P.; Klein, M. L.; Devane, R. H.; Aqad, E.; Rosen, B. M.; Argintaru, A. O.; Sienkowska, M. J.; Rissanen, K.; Nummelin, S.; Ropponen, J. Self-Assembly of Janus Dendrimers into Uniform Dendrimersomes and Other Complex Architectures. *Science (80-.).* **2010**, *328* (May), 1009−1015.

(4) Caminade, A. M.; Laurent, R.; Delavaux-Nicot, B.; Majoral, J. P. Janus" Dendrimers: Syntheses and Properties. *New J. Chem.* **2012**, *36* (2), 217−226.

(5) Wilner, S. E.; Xiao, Q.; Graber, Z. T.; Sherman, S. E.; Percec, V.; Baumgart, T. Dendrimersomes Exhibit Lamellar-to-Sponge Phase Transitions. *Langmuir* **2018**, *34* (19), 5527−5534.

(6) Zhang, S.; Sun, H. J.; Hughes, A. D.; Draghici, B.; Lejnieks, J.; Leowanawat, P.; Bertin, A.; Otero De Leon, L.; Kulikov, O. V.; Chen, Y.; Pochan, D. J.; Heiney, P. A.; Percec, V. Single-Single" Amphiphilic Janus Dendrimers Self-Assemble Into Uniform Dendrimersomes With Predictable Size. *ACS Nano* **2014**, *8* (2), 1554−1565.

(7) Sherman, S. E.; Xiao, Q.; Percec, V. Mimicking Complex Biological Membranes and Their Programmable Glycan Ligands with Dendrimersomes and Glycodendrimersomes. *Chem. Rev.* **2017**, *117* (9), 6538−6631.

(8) Sun, H. J.; Zhang, S.; Percec, V. From Structure to Function via Complex Supramolecular Dendrimer Systems. *Chem. Soc. Rev.* **2015**, *44* (12), 3900−3923.

(9) Tomalia, D. A. Dendritic Effects: Dependency of Dendritic Nano-Periodic Property Patterns on Critical Nanoscale Design Parameters (CNDPs). *New J. Chem.* **2012**, *36* (2), 264−281.

(10) Park, C.; Lee, J.; Kim, C. Functional Supramolecular Assemblies Derived from Dendritic Building Blocks. *Chem. Commun.* **2011**, *47* (44), 12042−12056.

(11) Frechet, J. M. J. Dendrimers and Other Dendritic Macromolecules: From. *J. Polym. Sci. Part A Polym. Chem.* **2003**, *41*, 3713−3725.

(12) Tomalia, D. A. Supramolecular Chemistry: Fluorine Makes a Difference. *Nat. Mater.* **2003**, *2* (11), 711−712.

(13) Percec, V.; Glodde, M.; Johansson, G.; Balagurusamy, V. S. K.; Heiney, P. A. Transformation of a Spherical Supramolecular Dendrimer into a Pyramidal Columnar Supramolecular Dendrimer Mediated by the Fluorophobic Effect. *Angew. Chem. Int. Ed* **2003**, *42*, 4338−4342.

(14) Berger, R.; Resnati, G.; Metrangolo, P.; Weber, E.; Hulliger, J. Organic Fluorine Compounds: A Great Opportunity for Enhanced Materials Properties. *Chem. Soc. Rev.* **2011**, *40* (7), 3496−3508.

(15) Gladysz, J. A.; Jurisch, M. *Structural, Physical, and Chemical Properties of Fluorous Compounds*; Horváth, I., Ed.; Springer: Berlin, 2011.

(16) Barthel-Rosa, L. P.; Gladysz, J. A. Chemistry in Fluorous Media: A User's Guide to Practical Considerations in the Application of Fluorous Catalysts and Reagents. *Coord. Chem. Rev.* **1999**, *190−192*, 587−605.

(17) Krafft, M. P. Fluorocarbons and Fluorinated Amphiphiles in Drug Delivery and Biomedical Research. *Adv. Drug Delivery Rev.* **2001**, *47* (2−3), 209−228.

(18) Krafft, M. P. Highly Fluorinated Compounds Induce Phase Separation in, and Nanostructuration of Liquid Media. Possible Impact on, and Use in Chemical Reactivity Control. *J. Polym. Sci. Part A Polym. Chem.* **2006**, *44*, 4251−4258.

(19) Shiyanovskaya, I.; Singer, K. D.; Percec, V.; Bera, T. K.; Miura, Y.; Glodde, M.; et al. Self-Organization of Supramolecular Helical Dendrimers into Complex Electronic Materials. *Nature* **2002**, *419*, 384−387.

(20) Percec, V.; Aqad, E.; Peterca, M.; Imam, M. R.; Glodde, M.; Bera, T. K.; Miura, Y.; Balagurusamy, V. S. K.; Ewbank, P. C.; Würthner, F.; Heiney, P. A. Self-Assembly of Semifluorinated Minidendrons Attached to Electron-Acceptor Groups into Pyramidal Columns. *Chem. - A Eur. J.* **2007**, *13* (12), 3330−3345.

(21) Rosen, B. M.; Percec, V. Single-Electron Transfer and Single-Electron Transfer Degenerative Chain Transfer Living Radical Polymerization. *Chem. Rev.* **2009**, *109* (11), 5069−5119.

(22) Wilson, C. J.; Wilson, D. A.; Feiring, A. E.; Percec, V. Disassembly via an Environmentally Friendly and Efficient Fluorous Phase Constructed with Dendritic Architectures. *J. Polym. Sci. Part A Polym. Chem.* **2010**, *48* (11), 2498−2508.

(23) Wu, Y. C.; Leowanawat, P.; Sun, H. J.; Partridge, B. E.; Peterca, M.; Graf, R.; Spiess, H. W.; Zeng, X.; Ungar, G.; Hsu, C. S.; Heiney, P. A.; Percec, V. Complex Columnar Hexagonal Polymorphism in Supramolecular Assemblies of a Semifluorinated Electron-Accepting Naphthalene Bisimide. *J. Am. Chem. Soc.* **2015**, *137* (2), 807−819.

(24) Ho, M. S.; Partridge, B. E.; Sun, H. J.; Sahoo, D.; Leowanawat, P.; Peterca, M.; Graf, R.; Spiess, H. W.; Zeng, X.; Ungar, G.; Heiney, P. A.; Hsu, C. S.; Percec, V. Screening Libraries of Semifluorinated Arylene Bisimides to Discover and Predict Thermodynamically Controlled Helical Crystallization. *ACS Comb. Sci.* **2016**, *18* (12), 723−739.

(25) Hernández-Ainsa, S.; Barberá, J. Fluorinated Liquid Crystalline Dendrimers. *J. Fluor. Chem.* **2015**, *177*, 37−45.

(26) Percec, V.; Glodde, M.; Peterca, M.; Rapp, A.; Schnell, I.; Spiess, H. W.; Bera, T. K.; Miura, Y.; Balagurusamy, V. S. K.; Aqad, E.; Heiney, P. A. Self-Assembly of Semifluorinated Dendrons Attached to Electron-Donor Groups Mediates Their π-Stacking via a Helical Pyramidal Column. *Chem. - A Eur. J.* **2006**, *12* (24), 6298−6314.

(27) Dukeson, D. R.; Ungar, G.; Balagurusamy, V. S. K.; Percec, V.; Johansson, G. A.; Glodde, M. Application of Isomorphous Replacement in the Structure Determination of a Cubic Liquid Crystal Phase and Location of Counterions. *J. Am. Chem. Soc.* **2003**, *125* (51), 15974−15980.

(28) Xiao, Q.; Rubien, J. D.; Wang, Z.; Reed, E. H.; Hammer, D. A.; Sahoo, D.; Heiney, P. A.; Yadavalli, S. S.; Goulian, M.; Wilner, S. E.; Baumgart, T.; Vinogradov, S. A.; Klein, M. L.; Percec, V. Self-Sorting and Coassembly of Fluorinated, Hydrogenated, and Hybrid Janus Dendrimers into Dendrimersomes. *J. Am. Chem. Soc.* **2016**, *138* (38), 12655−12663.

(29) Xiao, Q.; Sherman, S. E.; Wilner, S. E.; Zhou, X.; Dazen, C.; Baumgart, T.; Reed, E. H.; Hammer, D. A.; Shinoda, W.; Klein, M. L.; Percec, V. Janus Dendrimersomes Coassembled from Fluorinated, Hydrogenated, and Hybrid Janus Dendrimers as Models for Cell

https://doi.org/10.1021/acs.macromol.2c00129
Macromolecules 2022, 55, 2486−2496

Fusion and Fission. *Proc. Natl. Acad. Sci. U. S. A.* **2017**, *114* (34), E7045−E7053.
(30) Percec, V.; Imam, M. R.; Bera, T. K.; Balagurusamy, V. S. K.; Peterca, M.; Heiney, P. A. Self-Assembly of Semifluorinated Janus-Dendritic Benzamides into Bilayered Pyramidal Columns**. *Angew. Chem., Int. Ed.* **2005**, *44*, 4739−4745.
(31) Percec, V.; Imam, M. R.; Peterca, M.; Leowanawat, P. Self-Organizable Vesicular Columns Assembled from Polymers Dendronized with Semifluorinated Janus Dendrimers Act as Reverse Thermal Actuators. *J. Am. Chem. Soc.* **2012**, *134* (9), 4408−4420.
(32) Torre, P.; Xiao, Q.; Buzzacchera, I.; Sherman, S. E.; Rahimi, K.; Kostina, N. Y.; Rodriguez-Emmenegger, C.; Möller, M.; Wilson, C. J.; Klein, M. L.; Good, M. C.; Percec, V. Encapsulation of Hydrophobic Components in Dendrimersomes and Decoration of Their Surface with Proteins and Nucleic Acids. *Proc. Natl. Acad. Sci. U. S. A.* **2019**, *116* (31), 15378−15385.
(33) Lv, J.; Cheng, Y. Fluoropolymers in Biomedical Applications: State-of-the-Art and Future Perspectives. *Chem. Soc. Rev.* **2021**, *50* (9), 5435−5467.
(34) Jiang, J.; Zhang, G.; Wang, Q.; Zhang, Q.; Zhan, X.; Chen, F. Novel Fluorinated Polymers Containing Short Perfluorobutyl Side Chains and Their Super Wetting Performance on Diverse Substrates. *ACS Appl. Mater. Interfaces* **2016**, *8* (16), 10513−10523.
(35) Zhang, Z.; Shen, W.; Ling, J.; Yan, Y.; Hu, J.; Cheng, Y. The Fluorination Effect of Fluoroamphiphiles in Cytosolic Protein Delivery. *Nat. Commun.* **2018**, *9* (1), 1377 DOI: 10.1038/s41467-018-03779-8.
(36) Kostina, N. Y.; Rahimi, K.; Xiao, Q.; Haraszti, T.; Dedisch, S.; Spatz, J. P.; Schwaneberg, U.; Klein, M. L.; Percec, V.; Möller, M.; Rodriguez-Emmenegger, C. Membrane-Mimetic Dendrimersomes Engulf Living Bacteria via Endocytosis. *Nano Lett.* **2019**, *19* (8), 5732−5738.
(37) Celentano, W.; Neri, G.; Distante, F.; Li, M.; Messa, P.; Chirizzi, C.; Chaabane, L.; De Campo, F.; Metrangolo, P.; Baldelli Bombelli, F.; Cellesi, F. Design of Fluorinated Hyperbranched Polyether Copolymers for 19F MRI Nanotheranostics. *Polym. Chem.* **2020**, *11* (24), 3951−3963.
(38) Chowdhury, M. S.; Zheng, W.; Kumari, S.; Heyman, J.; Zhang, X.; Dey, P.; Weitz, D. A.; Haag, R. Dendronized Fluorosurfactant for Highly Stable Water-in-Fluorinated Oil Emulsions with Minimal Inter-Droplet Transfer of Small Molecules. *Nat. Commun.* **2019**, *10* (1), 4546 DOI: 10.1038/s41467-019-12462-5.
(39) Garcia-Bernabé, A.; Krämer, M.; Olàh, B.; Haag, R. Syntheses and Phase-Transfer Properties of Dendritic Nanocarriers That Contain Perfluorinated Shell Structures. *Chem. - A Eur. J.* **2004**, *10* (11), 2822−2830.
(40) Wagner, O.; Zieringer, M.; Duncanson, W. J.; Weitz, D. A.; Haag, R. Perfluoroalkyl-Functionalized Hyperbranched Polyglycerol as Pore Forming Agents and Supramolecular Hosts in Polymer Microspheres. *Int. J. Mol. Sci.* **2015**, *16* (9), 20183−20194.
(41) Krafft, M. P.; Riess, J. G. Per- and Polyfluorinated Substances (PFASs): Environmental Challenges. *Curr. Opin. Colloid Interface Sci.* **2015**, *20* (3), 192−212.
(42) Bowman, J. S. Fluorotechnology Is Critical to Modern Life: The FluoroCouncil Counterpoint to the Madrid Statement. *Environ. Health Perspect.* **2015**, *123* (5), A107−A111.
(43) Dichiarante, V.; Milani, R.; Metrangolo, P. Natural Surfactants towards a More Sustainable Fluorine Chemistry. *Green Chem.* **2018**, *20* (1), 13−27.
(44) Schuster, T.; Krumpfer, J. W.; Schellenberger, S.; Friedrich, R.; Klapper, M.; Müllen, K. Effects of Chemical Structure on the Dynamic and Static Surface Tensions of Short-Chain, Multi-Arm Nonionic Fluorosurfactants. *J. Colloid Interface Sci.* **2014**, *428*, 276−285.
(45) Dichiarante, V.; Martinez Espinoza, M. I.; Gazzera, L.; Vuckovac, M.; Latikka, M.; Cavallo, G.; Raffaini, G.; Oropesa-Nunez, R.; Canale, C.; Dante, S.; Marras, S.; Carzino, R.; Prato, M.; Ras, R. H. A.; Metrangolo, P. A Short-Chain Multibranched Perfluoroalkyl Thiol for More Sustainable Hydrophobic Coatings. *ACS Sustain. Chem. Eng.* **2018**, *6* (8), 9734−9743.
(46) Dichiarante, V.; Tirotta, I.; Catalano, L.; Terraneo, G.; Raffaini, G.; Chierotti, M. R.; Gobetto, R.; Baldelli Bombelli, F.; Metrangolo, P. Superfluorinated and NIR-Luminescent Gold Nanoclusters. *Chem. Commun.* **2017**, *53* (3), 621.
(47) Tedeschi, G.; Guzman-Puyol, S.; Ceseracciu, L.; Benitez, J. J.; Goldoni, L.; Koschella, A.; Heinze, T.; Cavallo, G.; Dichiarante, V.; Terraneo, G.; Athanassiou, A.; Metrangolo, P.; Heredia-Guerrero, J. A. Waterproof-Breathable Films from Multi-Branched Fluorinated Cellulose Esters. *Carbohydr. Polym.* **2021**, *271*, 118031.
(48) Taraban, M. B.; Deredge, D. J.; Smith, M. E.; Briggs, K. T.; Li, Y.; Jiang, Z. X.; Wintrode, P. L.; Yu, Y. B. Monitoring Dendrimer Conformational Transition Using 19F and $1H_2O$ NMR. *Magn. Reson. Chem.* **2019**, *57* (10), 861−872.
(49) Liu, X.; Yuan, Y.; Bo, S.; Li, Y.; Yang, Z.; Zhou, X.; Chen, S.; Jiang, Z. X. Monitoring Fluorinated Dendrimer-Based Self-Assembled Drug-Delivery Systems with 19F Magnetic Resonance. *Eur. J. Org. Chem.* **2017**, *2017* (30), 4461−4468.
(50) Taraban, M. B.; Yu, L.; Feng, Y.; Jouravleva, E. V.; Anisimov, M. A.; Jiang, Z. X.; Yu, Y. B. Conformational Transition of a Non-Associative Fluorinated Amphiphile in Aqueous Solution. *RSC Adv.* **2014**, *4* (97), 54565−54575.
(51) Jiang, Z. X.; Liu, X.; Jeong, E. K.; Yu, Y. B. Symmetry-Guided Design and Fluorous Synthesis of a Stable and Rapidly Excreted Imaging Tracer For19F MRI. *Angew. Chemie - Int. Ed.* **2009**, *48* (26), 4755−4758.
(52) Medina, S. H.; El-Sayed, M. E. H. Dendrimers as Carriers for Delivery of Chemotherapeutic Agents. *Chem. Rev.* **2009**, *109* (7), 3141−3157.
(53) Peterca, M.; Percec, V.; Leowanawat, P.; Bertin, A. Predicting the Size and Properties of Dendrimersomes from the Lamellar Structure of Their Amphiphilic Janus Dendrimers. *J. Am. Chem. Soc.* **2011**, *133* (50), 20507−20520.
(54) Fedeli, E.; Lancelot, A.; Serrano, J. L.; Calvo, P.; Sierra, T. Self-Assembling Amphiphilic Janus Dendrimers: Mesomorphic Properties and Aggregation in Water. *New J. Chem.* **2015**, *39* (3), 1960−1967.
(55) Núñez, E.; Ferrando, C.; Malmström, E.; Claesson, H.; Werner, P. E.; Gedde, U. W. Crystal Structure, Melting Behaviour and Equilibrium Melting Point of Star Polyesters with Crystallisable Poly(ε-Caprolactone) Arms. *Polymer (Guildf).* **2004**, *45* (15), 5251−5263.
(56) Zeng, X.; Poppe, S.; Lehmann, A.; Prehm, M.; Chen, C.; Liu, F.; Lu, H.; Ungar, G.; Tschierske, C. Liquid Crystals A Self-Assembled Bicontinuous Cubic Phase with a Single-Diamond Network. *Angew. Chem. Int. Ed* **2019**, *58*, 7375−7379.
(57) Poppe, S.; Chen, C.; Liu, F.; Tschierske, C. A Skeletal Double Gyroid Formed by Single Coaxial Bundles of Catechol Based Bolapolyphiles. *Chem. Commun.* **2018**, *54*, 11196−11199.
(58) Corvis, Y.; Négrier, P.; Soulestin, J.; Espeau, P. New Melting Data of the Two Polymorphs of Prednisolone. *J. Phys. Chem. B* **2016**, *120* (41), 10839−10843.
(59) Zhao, J.; Sun, Y.; Men, Y. Melt Temperature and Initial Polymorphs Dependencies of Polymorphs Selection during Subsequent Crystallization in Propylene-Ethylene Random Copolymer. *Ind. Eng. Chem. Res.* **2017**, *56* (1), 198−205.
(60) Tuuttila, T.; Lahtinen, M.; Kuuloja, N.; Huuskonen, J.; Rissanen, K. Synthesis and Thermal Behavior of Janus Dendrimers, Part 1. *Thermochim. Acta* **2010**, *497* (1−2), 101−108.
(61) Preslar, A. T.; Tantakitti, F.; Park, K.; Zhang, S.; Stupp, S. I.; Meade, T. J. 19F Magnetic Resonance Imaging Signals from Peptide Amphiphile Nanostructures Are Strongly Affected by Their Shape. *ACS Nano* **2016**, *10* (8), 7376−7384.
(62) Yu, J.; Sun, D.; Ai, H.; Wang, X.; Zhai, L. Novel Mechanism for Nanotube Formation from Vesicle: A Transition Induced by the Rearrangement of Molecular Pairs. *Colloids Surfaces A Physicochem. Eng. Asp.* **2013**, *422*, 148−154.
(63) Ramanathan, M.; Shrestha, L. K.; Mori, T.; Ji, Q.; Hill, J. P.; Ariga, K. Amphiphile Nanoarchitectonics: From Basic Physical

Chemistry to Advanced Applications. *Phys. Chem. Chem. Phys.* **2013**, *15*, 10580−10611.
(64) Tirotta, I.; Mastropietro, A.; Cordiglieri, C.; Gazzera, L.; Baggi, F.; Baselli, G.; Bruzzone, M. G.; Zucca, I.; Cavallo, G.; Terraneo, G.; Bombelli, F. B.; Metrangolo, P.; Resnati, G. A Superfluorinated Molecular Probe for Highly Sensitive in Vivo 19 F - MRI. *J. Am. Chem. Soc.* **2014**, *136*, 8524−8527.
(65) Huynh, A. M.; Müller, A.; Kessler, S. M.; Henrikus, S.; Hoffmann, C.; Kiemer, A. K.; Bücker, A.; Jung, G. Small BODIPY Probes for Combined Dual 19 F MRI and Fluorescence Imaging. *ChemMedChem.* **2016**, *11*, 1568−1575.
(66) Tirotta, I.; Dichiarante, V.; Pigliacelli, C.; Cavallo, G.; Terraneo, G.; Bombelli, F. B.; Metrangolo, P.; Resnati, G. ^{19}F Magnetic Resonance Imaging (MRI): From Design of Materials to Clinical Applications. *Chem. Rev.* **2015**, *115* (2), 1106.
(67) Groot, R. D.; Rabone, K. L. Mesoscopic Simulation of Cell Membrane Damage, Morphology Change and Rupture by Nonionic Surfactants. *Biophys. J.* **2001**, *81* (2), 725−736.
(68) Arai, N.; Yasuoka, K.; Zeng, X. C. Self-Assembly of Janus Oligomers into Onion-like Vesicles with Layer-by-Layer Water Discharging Capability: A Minimalist Model. *ACS Nano* **2016**, *10* (8), 8026−8037.
(69) Chang, H. Y.; Lin, Y. L.; Sheng, Y. J.; Tsao, H. K. Structural Characteristics and Fusion Pathways of Onion-like Multilayered Polymersome Formed by Amphiphilic Comb-like Graft Copolymers. *Macromolecules* **2013**, *46* (14), 5644−5656.
(70) Ivnitski, D.; Amit, M.; Silberbush, O.; Atsmon-Raz, Y.; Nanda, J.; Cohen-Luria, R.; Miller, Y.; Ashkenasy, G.; Ashkenasy, N. The Strong Influence of Structure Polymorphism on the Conductivity of Peptide Fibrils. *Angew. Chemie - Int. Ed.* **2016**, *55* (34), 9988−9992.
(71) Gillissen, M. A. J.; Koenigs, M. M. E.; Spiering, J. J. H.; Vekemans, J. A. J. M.; Palmans, A. R. A.; Voets, I. K.; Meijer, E. W. Triple Helix Formation in Amphiphilic Discotics: Demystifying Solvent Effects in Supramolecular Self-Assembly. *J. Am. Chem. Soc.* **2014**, *136* (1), 336−343.
(72) Po, C.; Tam, A. Y. Y.; Wong, K. M. C.; Yam, V. W. W. Supramolecular Self-Assembly of Amphiphilic Anionic Platinum(II) Complexes: A Correlation between Spectroscopic and Morphological Properties. *J. Am. Chem. Soc.* **2011**, *133* (31), 12136−12143.
(73) Baldelli Bombelli, F.; Metrangolo, P.; Cavallo, G.; Bono, N.; Candiani, G.; Rosati, M.; Pinter Lauria, G.; Marcuzzo, S. (Inventors) ; Politecnico di Milanoand Fondazione IRCCS IstitutoNeurologico Carlo Besta, (Owners) ; IT102022000004496, 9 March 2022.

https://doi.org/10.1021/acs.macromol.2c00129
Macromolecules 2022, 55, 2486−2496